Climate: The Elements

JOHN A. T. BYE, ROLAND A. D. BYRON-SCOTT, AND ADRIAN H. GORDON

Flinders Institute for Atmospheric and Marine Sciences, Flinders University of South Australia, Adelaide, Australia

(Manuscript received 20 July 1994, in final form 6 December 1995)

ABSTRACT

The authors present an analytical climate model, which has the features that (i) the atmosphere is a simple oscillator for all periods $\geq$ 1 year, (ii) the ocean stores heat, (iii) the ocean exchanges momentum with the atmosphere, and (iv) random forcing exists due to atmospheric thermodynamics and oceanic dynamics. The piecewise analytical integration of coupled linear equations for sea temperature, air–sea temperature difference, and air–sea velocity difference generates experimental climates. The exchange parameters of the algorithm, except for the exchange coefficient for heat with the deep ocean, are calibrated to the observed climate using the annual cycle, and random forcing is applied over intervals of one year. The atmospheric random forcing leads to bounded random walks, the extent of which increases as the exchange coefficient with the deep ocean decreases, and the oceanic random forcing generates a stationary response. It is found that the observed statistics of the global temperature series can be reproduced by either a relatively large heat exchange coefficient with the deep ocean and little oceanic variability or a smaller exchange coefficient with a larger oceanic variability. Plausible exchange coefficient values imply random walk lengths of at least a century-long timescale.

1. Introduction

In a recent investigation (Gordon and Bye 1993), we extracted statistics from the global temperature series with the aim of determining which part of the signal was due to random processes. It was found that a useful diagnostic was the transition ratio (the mean ratio of the interannual temperature difference in successive pairs of years). Here we construct a climatic algorithm that reproduces the observed transition ratio and examine what insights it offers on the global climate.

In the literature, many and varied climate models have been considered (IPCC 1992), which are sufficiently simple that a rapid examination of their predictions can be made over a comprehensive parameter space. This is precluded in coupled general circulation models owing to computational limitations. Our model lies in this category, and it is also linear, all nonlinear processes being hidden in the specification of the random forcing. This stochastic approach to climatic variability was introduced by Hasselmann (1976). We consider carefully the physical nature of the stochastic forcing. In particular, a clear distinction is made between forcing due to the atmospheric thermodynamics and that due to oceanic dynamics. The algorithm takes no explicit account of the hydrological cycle—that is, ice, water vapor, evaporation rainfall, and salinity interactions—and relies solely on heat and momentum equations, but it is reasonable to regard the random forcing as arising from the neglected hydrological regime.

2. The model

Figure 1 illustrates the model, which consists of an atmosphere that oscillates and is supported by a mixed layer that interacts with a deep ocean of infinite or finite extent. The system is driven by radiation entering the top of the atmosphere, and it simulates climate on annual and interannual timescales. The elements of the model are described in the sections that follow.

a. The atmospheric oscillations

Atmospheric oscillations are maintained by exchange of potential and kinetic energy, which are represented by the equations

$$\frac{d\phi_0}{dt} - \omega U_0 = 0 \tag{1}$$

and

$$\frac{dU_0}{dt} + \omega\phi_0 = 0, \tag{2}$$

in which ϕ_0 is the air temperature relative to the mean air temperature; U_0 is a normalized air velocity, which for brevity will be called, respectively, the air temper-

Corresponding author address: Dr. John A. T. Bye, Flinders Institute for Atmospheric and Marine Sciences, Flinders University of South Australia, GPO Box 2100, Adelaide 5001, Australia.

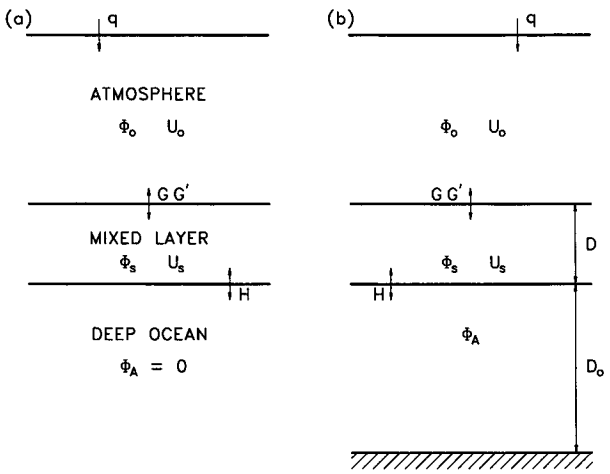

FIG. 1. Cartoon of the coupled ocean–atmosphere model: a) the equilibrium model and (b) the transient model.

ature and the surface wind; t is in years; and $\omega = 2\pi/T_0$ is the angular frequency of the atmospheric oscillation of period T_0 years.

In the sign convention adopted for the velocity, U_0 is positive for a flow from a cold to a hot region. That is, $dU_0/dt > 0$, if $\phi_0 < 0$.

The wave solution of (1) and (2) is

$$\phi_0 = c_0 \cos(\omega t - g_0) \tag{3}$$

and

$$U_0 = -c_0 \sin(\omega t - g_0), \tag{4}$$

where c_0 and g_0 are constants, which represents an oscillation in which U_0 is out of phase with ϕ_0. The homogeneous formulation of (1) and (2) implies that the atmosphere is assumed to be (i) transparent to radiation—that is, there is no storage of heat—and (ii) dissipative—that is, there is no storage of momentum. The assumptions are discussed fully in section 2d.

b. Transformation to an oceanic reference frame

The atmospheric oscillation defined relative to the earth occurs to a significant extent over the oceans, which cover about two-thirds of the earth's surface. Transformation of (1) and (2) to a reference frame relative to the ocean is achieved by defining the variables

$$\psi = \phi_0 - \phi_s$$

and

$$\lambda = U_0 - U_s,$$

where ψ is the air–sea temperature difference, ϕ_s is the sea surface temperature, and λ is the surface wind (U_0) relative to the surface current (U_s). In this oceanic reference frame, the relative temperature and velocity are forced by the sea surface temperature and the surface current. Thus,

$$\frac{d\psi}{dt} - \omega\lambda = -\frac{d\phi_s}{dt} + \omega U_s, \tag{5}$$

and

$$\frac{d\lambda}{dt} + \omega\psi = -\frac{dU_s}{dt} - \omega\phi_s. \tag{6}$$

c. The mixed layer interactions

The surface oceanic properties will be assumed to be controlled by mixed layer budgets of heat and momentum. The thermal budget is represented by the equation

$$\frac{d\phi_s}{dt} = G(\phi_0 - \phi_s) - H\phi_s, \tag{7}$$

where the coefficients G and H are Newtonian exchange coefficients for the air–mixed layer and mixed layer–deep ocean transfers, respectively, and the deep ocean temperature (ϕ_A) is the mean air temperature.

This formulation, in which the deep ocean is thermally passive, we call the equilibrium model (Fig. 1a). It is extended to include an active deep ocean of finite heat capacity, which is called the transient model (Fig. 1b), in section 6.

In reality, the mean deep ocean temperature is less than the mean air temperature, due to the effect of salinity on the structure of the water column. Here we assume that this hydrological regime, which may determine the magnitude of the exchange coefficient (H), is prescribed and consider only the effects of short-term variability, in which H is assumed to be a constant. Hence, it is reasonable to interpret $\phi_A = 0$ as a reference deep ocean temperature and ϕ_A as a deep ocean temperature anomaly in the same way that ϕ_0 and ϕ_s are air temperature and sea surface temperature anomalies, with respect to the mean air temperature.

The dynamic balance is represented by the equation

$$\frac{dU_s}{dt} = G'(U_0 - sU_s), \tag{8}$$

in which G' is the momentum exchange coefficient with the atmosphere, and the coefficient s is the understress coefficient. For viscous coupling of the ocean and atmosphere, $s = 1$, and for inertial coupling, which occurs in the presence of gravity waves, $s = 1/\epsilon$ where $\epsilon = (\rho_a/\rho)^{1/2}$, ρ_a being the density of air and ρ the density of seawater (Bye 1988, 1995).

This pair of equations can be expressed in similar form by substituting for ψ and λ:

$$\frac{d\phi_s}{dt} = G\psi - H\phi_s, \tag{9}$$

and

$$\frac{dU_s}{dt} = G'\lambda - G'\alpha U_s, \tag{10}$$

where $\alpha = s - 1$. The interpretation of these equations is that the mixed layer is in thermal equilibrium ($d\phi_s/dt = 0$) if $G\psi = H\phi_s$; that is, the rate of gain of heat from the atmosphere (the surface heat flux) is equal to the rate of loss of heat to the deep ocean (the interfacial heat flux). In nonequilibrium situations, the net heat flux causes ϕ_s to change at a rate that is inversely proportional to the mixed layer depth, which is a free parameter.

Similarly, the mixed layer is in dynamical equilibrium ($dU_s/dt = 0$) if $G'\lambda = G'\alpha U_s$; that is, the rate of gain of momentum due to the shear between the surface wind and current is equal to the rate of loss. According to (8), this equilibrium is equivalent to $G'U_0 = G'sU_s$—that is, a balance between the wind stress and the understress. Momentum loss to the deep ocean by the interfacial stress (Johnson and Bryden 1989) may also be included by increasing s. In nonequilibrium conditions, the net shearing stress accelerates (or decelerates) the mixed layer. Upon substituting (9) and (10) into (5) and (6), we obtain

$$\frac{d\psi}{dt} + G\psi - \omega\lambda = H\phi_s + \omega U_s \tag{11}$$

and

$$\frac{d\lambda}{dt} + G'\lambda + \omega\psi = -\omega\phi_s + G'\alpha U_s. \tag{12}$$

d. The atmospheric conditions

The assumptions (i) and (ii) of section 2a can be implemented to obtain expressions for ϕ_s and U_s as follows.

1) THE TRANSPARENT ATMOSPHERE

The transparent atmosphere directly yields the equation

$$q = B\psi, \tag{13}$$

where q is the radiation entering the top of the atmosphere and B is an atmospheric heat exchange coefficient. Upon substituting in (7), we obtain

$$\frac{d\phi_s}{dt} + H\phi_s = \frac{G}{B}q, \tag{14}$$

which can be solved for ϕ_s for any specified radiative forcing.

2) THE DISSIPATIVE ATMOSPHERE

The dissipative atmosphere yields the relation

$$F = c\lambda, \tag{15}$$

in which F is the relative stress and c is a Rayleigh drag coefficient. Upon substituting in (15), (8) yields

$$\frac{dU_s}{dt} + \alpha G'U_s = \frac{G'F}{c}, \tag{16}$$

which can be solved for U_s for any F.

3. The solutions

The pair of coupled equations (11) and (12) together with the auxiliary equations (14) and (16) constitute the equilibrium climate model. We consider solutions for cyclic and random forcing and assume throughout that G, G', H, B, and c are all constants. The assumption that G, G', and H are constants neglects the effects of static stability on the exchange processes.

a. The annual cycle

The annual radiative cycle is represented by the harmonic function

$$q = q_0 \cos 2\pi t, \tag{17}$$

where the time origin occurs at the summer solstice, q_0 is the amplitude of the radiative cycle, and $\omega = 2\pi$ ($T_0 = 1$ yr and t is in years). Upon substituting (17) into (14), we obtain

$$\frac{d\phi_s}{dt} + H\phi_s = \frac{G}{B}q_0 \cos 2\pi t, \tag{18}$$

the solution of which is,

$$\phi_s = a_s \cos 2\pi t + b_s \sin 2\pi t, \tag{19}$$

where

$$a_s = \frac{\left(\frac{G}{B}q_0\right)H}{[(2\pi)^2 + H^2]}$$

and

$$b_s = \frac{\left(\frac{G}{B}q_0\right)2\pi}{[(2\pi)^2 + H^2]}.$$

Upon substituting in (13), we obtain

$$\phi_0 = a_0 \cos 2\pi t + b_0 \sin 2\pi t, \tag{20}$$

where

$$a_0 = \frac{q_0}{B} + a_s$$

and

$$b_0 = b_s.$$

Upon expressing these results in phase and amplitude form, we have

$$\phi_s = c_s \cos(2\pi t - g_s) \tag{21}$$

and

$$\phi_0 = c_0 \cos(2\pi t - g_0), \tag{22}$$

where

$$c_s = \frac{q_0}{B} \frac{G}{[(2\pi)^2 + H^2]^{1/2}}, \quad g_s = \tan^{-1}\left(\frac{2\pi}{H}\right)$$

and

$$c_0 = \frac{q_0}{B}\left[\frac{(2\pi)^2 + (G+H)^2}{(2\pi)^2 + H^2}\right]^{1/2},$$

$$g_0 = \tan^{-1}\left[\frac{2\pi G}{(2\pi)^2 + H^2 + GH}\right].$$

The lag of the seasons (L), defined as the lag of the air temperature cycle over the radiation cycle, converted to months is $6g_0/\pi$.

The corresponding result for the surface wind is

$$U_0 = c_0 \cos(2\pi t - k_0), \tag{23}$$

where $k_0 = g_0 - \pi/2$, and the surface current is obtained by substituting for U_0 and solving (8), from which we obtain

$$U_s = A_s \cos 2\pi t + B_s \sin 2\pi t, \tag{24}$$

where

$$A_s = \frac{G'(sG'b_0 + 2\pi a_0)}{(2\pi)^2 + (sG')^2}$$

and

$$B_s = \frac{G'(-sG'a_0 + 2\pi b_0)}{(2\pi)^2 + (sG')^2}.$$

Alternatively,

$$U_s = d_s \cos(2\pi t - k_s), \tag{25}$$

in which

$$d_s = \frac{c_0 G'}{[(2\pi)^2 + (sG')^2]^{1/2}}$$

and

$$k_s = k_0 + k',$$

where $k' = \tan^{-1}(2\pi/sG')$, such that the lag of the current over the wind (M) is $6k'/\pi$. The velocities also determine the relative stress from (15) and yield the harmonic relation

$$F = c(U_0 - U_s). \tag{26}$$

The cyclic solution represents a deterministic system in which all the properties can be forecast from the radiation cycle, including the momentum exchange across the sea surface. It can be used to estimate the parameters that are to be used in the random forcing solutions, which for the linear model are added to the cyclic solution to simulate the interannual climate variability.

b. The random response

Within the coupled system there also exist perturbations of the thermal and dynamical fields, which can be represented in a climate model by random fluctuations (Hasselmann 1976) in q and F of the form

$$q = iq_0 \tag{27}$$

and

$$F = jF_0, \tag{28}$$

in which i and j are drawn from random number distributions, i is expressed in the scale of the radiation forcing amplitude, and j is in the scale of F_0. Upon substituting (27) in (14) and integrating, we obtain

$$\phi_s = \epsilon + \phi_{s0} e^{-Ht}, \tag{29}$$

which consists of a random fluctuation due to i,

$$\epsilon = \frac{iq_0}{H}\frac{G}{B}(1 - e^{-Ht}),$$

and a transient response, $\phi_{s0}e^{-Ht}$, due to the sea surface temperature perturbation ϕ_{s0} at $t = 0$. Similarly, from (28) and (16) we obtain

$$U_s = \delta + U_{s0} e^{-G'\alpha t}, \tag{30}$$

where

$$\delta = \frac{jF_0}{c\alpha}(1 - e^{-\alpha G' t})$$

and $U_{s0}e^{-G'\alpha t}$ is the transient response due to the surface current perturbation U_{s0} at $t = 0$. Interannual climatic variability is generated by applying (29) and (30), substituted in (11) and (12), over a sequence of time intervals (t_n, t_{n+1}) where $t_{n+1} = t_n + h$, in each of which i and j are constants and $h = 1$ yr. This is an exact procedure, which constructs piecewise continuous solutions for ϕ_s and U_s and uses the solutions of (11) and (12) for ψ and λ as given in the appendix.

The relations (29) and (30) are of the form of a first-order autoregressive [AR(1)] scheme:

$$Y = A(1 - e^{-\theta t}) + Y_0 e^{-\theta t},$$

where A, Y_0, and θ are constants. The important parameter is the magnitude of the exponential term at the end of the time interval ($e^{-\theta h}$). For $\theta h \to 0$, the system transmits information from the previous interval without degradation. That is, it has a perfect memory of the previous variability, and

$$Y(h) \to A\theta h + Y_0. \tag{31}$$

Equation (31) is the random walk AR(1) limit, in which Y is augmented by the random number ($A\theta h$) at each time interval. For $\theta h \to \infty$, on the other hand,

$$Y \to A. \tag{32}$$

Equation (32) is the stationary AR(1) limit, in which the probability distribution of Y is identical to the distribution of the random forcing.

It is found (section 4) that for an annual interval, random radiative forcing tends toward the first limit ($\theta h \to 0$) and random dynamical forcing approximates the second limit ($\theta h \to \infty$). Thus, basically, the thermal field has a (bounded) random walk response and the dynamical field has an (almost) stationary response.

c. *The quasi-steady interannual response*

Working on the assumption that ψ and λ exhibit slowly varying excursions, (11) and (12) reduce approximately to the quasi-steady equations

$$\bar{\phi}_0 = \frac{\omega}{G}\bar{U}_0 + \left(1 + \frac{H}{G}\right)\phi_s \tag{33}$$

and

$$\bar{\phi}_0 = -\frac{\omega}{G'}\bar{U}_0 + \frac{G'(1+\alpha)}{\omega}U_s, \tag{34}$$

where $\bar{\phi}_0$ and $\bar{U}_0$ denote the quasi-steady estimates. The solutions of (33) and (34) for $\bar{\phi}_0$ and $\bar{U}_0$ are

$$\bar{\phi}_0 = \frac{G'[(H+G)\phi_s + \omega(1+\alpha)U_s]}{\omega^2 + GG'} \tag{35}$$

and

$$\bar{U}_0 = \frac{-\omega(H+G)\phi_s + GG'(1+\alpha)U_s}{\omega^2 + GG'}. \tag{36}$$

On the basis of the previous discussion, the maximum interannual excursions of ϕ_s are likely to be much greater than those of U_s, and hence (35) reduces approximately to the expression

$$\frac{\bar{\phi}_0}{\phi_s} = \frac{G'(H+G)}{\omega^2 + GG'}. \tag{37}$$

We discuss the implications of these relations (which are shown in section 5 to be an excellent approximation for interannual variability) in the two situations below.

1) $G'H < \omega^2$

Here, (37) indicates that $|\phi_s/\bar{\phi}_0| > 1$, such that the sea temperature anomaly would always be of greater magnitude than the air temperature anomaly. In this situation, during a cold anomaly ($\bar{\phi}_0 < 0$),

$$\phi_s < 0, \quad U_0 > 0, \quad \psi > 0, \quad q > 0, \quad \frac{\phi_s}{\phi_0} > 1,$$

in which there is a greater radiative input than in the air temperature anomaly, greater atmospheric stability, colder conditions with greatly reduced sea surface temperatures, and an enhanced monsoonal circulation. This scenario is consistent with a less stormy, more anticyclonic, drier environment with less cloudiness. On the other hand, during a warm anomaly ($\bar{\phi}_0 > 0$),

$$\phi_s > 0, \quad U_0 < 0, \quad \psi < 0, \quad q < 0, \quad \frac{\phi_s}{\phi_0} > 1,$$

in which there is a smaller radiative input, reduced atmospheric stability, warmer conditions with greatly increased sea surface temperatures, and reduced monsoonal activity. This situation corresponds with a more stormy, wetter environment with more cloudiness.

Hence, from (13) we have an *inverse* relation between sea surface temperature and radiation inputs, and the ω-climate regime exhibits a negative feedback regime in which the heating of the ocean's surface layer causes an increase in outgoing longwave radiation and vice versa. This is the typical situation for short-period climatic fluctuations.

2) $G'H > \omega^2$

Here, (37) indicates that $|\phi_s/\bar{\phi}_0| < 1$, such that the sea temperature anomaly would be always of lesser magnitude than the air temperature anomaly. In this situation, a cool anomaly would be accompanied by an increase in the outgoing longwave radiation and vice versa. This scenario occurs for longer-period climatic fluctuations, and in the limit of $\omega \to 0$, we obtain

$$\frac{\bar{\phi}_0}{\phi_s} = 1 + H/G,$$

in which the atmospheric temperature anomaly ($\bar{\phi}_0$) is maximized (with respect to ϕ_s). The atmospheric wind anomaly ($\bar{U}_0$), however, is maximized with respect to ϕ_s at the angular frequency $\omega_{\max} = (GG')^{1/2}$. For forcing by U_s, (35) and (36) indicate that the opposite response would occur, in which $\bar{\phi}_0$ would be maximized at $\omega_{\max} = (GG')^{1/2}$ and $\bar{U}_0$ for $\omega \to 0$.

d. *Random energy source distribution*

In the formulation of the climate algorithm, the period of the atmospheric oscillation is arbitrary. To simulate interannual climatic variability, which we consider to be the integrated response of ω climatic regimes of all periods $T_0 \geq T_{\min}$ where $T_{\min} = 2$ yr (such that $T_{\min}^{-1}$ is the interannual Nyquist frequency), we apply random forcing, which has the white noise distribution

$$\sigma_0^2 \propto T_0^{-1}, \quad T_0 \geq T_{\min}, \tag{38}$$

where σ_0 is the standard deviation of energy of periods $\leq T_0$. This distribution has the property that oscillations of all frequencies $T_0^{-1} \leq T_{\min}^{-1}$ are equally likely to be excited.

The method of implementing (38) for a specified sequence of frequencies is given in section 5b. The principle is that both the white noise interannual forcings [(27) and (28)] can be decomposed into a set of modes of periods ($T_0 \geqslant T_{\min}$) and arbitrary phases, which each satisfy the model equations and generate a corresponding ω-climatic regime.

4. Vital statistics

In order to make the simulations, the various constants of the climate model need to be specified. We omit the units of the exchange constants, which are yr^{-1} throughout.

a. The parameters G, G', and α

An important diagnostic is the lag of the seasons (L) (Byers 1974). Based on the assumption that the exchange constant for heat with the deep ocean (H) is much less than that with the atmosphere (G), (22) yields

$$G \sim \frac{1}{3} L\pi^2,$$

where L is in months. For $L \sim 1$ month, we obtain $G \sim 3$. Another estimate of G can be obtained from the mixed layer properties. For a depth of 100 m and an exchange constant of $\mu_H = 10^{-5}$ m s^{-1}, we obtain $G = 3.1$, which is in good agreement with the first estimate. For $G = 3$, we have from (21) and (22) that the ratio of the sea to air temperature anomalies is $c_s/c_0 \sim 0.43$. The exchange constant with the deep ocean (H) is not known a priori, and an important aim of section 5 is to estimate this.

For momentum, the exchange coefficient is

$$\mu_M \sim \frac{\rho_a K |\underline{u}_a|}{\rho_0},$$

in which $\underline{u}_a$ is a representative wind velocity and K is a drag coefficient. For $|\underline{u}_a| \sim 10$ m s^{-1} and $K \sim 2 \times 10^{-3}$, we find that $\mu_M \sim 2 \times 10^{-5}$ m s^{-1}. Hence, we estimate that $G' \sim 6$, such that the exchange of momentum occurs with twice the exchange (piston) velocity of heat. The lag of the current over the wind is $M \sim 2\frac{1}{2}$ days, compared to (25), and since $s \gg 1$, the ratio of the current to wind amplitudes ($d_s/c_0 \sim 1/s$) is 0.04.

For these parameters, $\omega_{\max} = 3\sqrt{2}$, and the corresponding period ($\pi 2^{1/2}/3$) is similar to the minimum period of the interannual forcing, $T_{\min} = 2$ yr. Thus the response to forcing by ϕ_s would be maximized for $\bar{\phi}_0$ at the low-frequency cutoff of the forcing, for $\bar{U}_0$ at the high-frequency cutoff, and vice versa for forcing by U_s.

The understress coefficient is assumed to have the value $\alpha = 25$ (see section 2c), such that for random forcing on an annual scale, $e^{-\alpha G' h} \sim 10^{-65}$. This value is so exceedingly small that for the simulation of *climate,* the precise value of α is unimportant. The forcing by the relative stress perturbation (jF_0) is clearly stationary, such that

$$U_s = \frac{jF_0}{c\alpha},$$

which as $|U_s| \ll |U_0|$, using (15), yields approximately,

$$U_s \sim \frac{jc_0}{\alpha}. \tag{39}$$

On the other hand, for random forcing on a diurnal scale, $e^{-\alpha G' h} \sim 0.7$, and hence the dynamical field would have a significant random walk behavior. This response would be characteristic of *weather,* which is not our concern here.

b. The parameter H

The method used to estimate H, which has a very important significance as it determines the boundedness of the random walks of the climate, is based on the analysis of the global temperature series (T_k) described in Gordon and Bye (1993).

The basic tool was to construct the mean amplitudes of the positive ($\Delta T_1 = T_{k+1} - T_k$, $\Delta T_1 > 0$) and negative ($\Delta T_1 < 0$) interannual transitions and the corresponding statistics for the following transitions ($\Delta T_2 = T_{k+2} - T_{k+1}$). From these statistics, the transition ratios $r_+ = \overline{\Delta T_2}/\overline{\Delta T_1}$, $\Delta T_1 > 0$; $r_- = \overline{\Delta T_2}/\overline{\Delta T_1}$, $\Delta T_1 < 0$; and

$$\bar{r} = \frac{1}{2}(r_+ + r_-)$$

can be determined. For a series constructed from a random distribution in the stationary limit, $\bar{r} = -0.5$, and in the random walk limit, $\bar{r} = 0$.

The global temperature series (Jones et al. 1991) was found to be characterized by the ratios

$$r_+ = -0.21, \quad r_- = -0.39,$$

and

$$\bar{r} = -0.29.$$

The difference between r_+ and r_- arises from the long-period trend of the series, but $\bar{r}$ is essentially independent of this trend. The representativeness of this value of $\bar{r}$ for the global temperature series was also strongly supported by the climate simulation of Manabe et al. (1991), which yielded $\bar{r} = -0.27$. The matching of $\bar{r}$ from the climate simulation with the observed value will be found to restrict the allowable range of H.

c. Random number distributions and random walk lengths

The random forcing used in the simulations is drawn from a random normal probability distribution of stan-

dard deviation (σ), which has the following well-known properties (Feller 1962).

1) The expected value of the absolute values is

$$E|x > 0| = \sqrt{\frac{2}{\pi}}\,\sigma.$$

The result enables the standard deviation (σ) to be estimated from the transitions of the series. For the global temperature series, we find (Gordon and Bye 1993) $\sigma = 0.125$ K. In the simulations, the amplitude of the air temperature cycle, $c_0 \sim 11$°C ($q_0/B = 10$ K), and the standard deviation of the normal distributions of i, σ_i, and j, σ_j were set such that ϕ_0 gave the observed standard deviation (σ). By (27), $\sigma_i q_0$ is the standard deviation of the radiation perturbation—for example, for $q_0 = 100$ W m^{-2} and $\sigma_i q_0 = 100\sigma_i$ W m^{-2}. By (39), the standard deviation of the normal distribution of j, σ_j, is the standard deviation of the ratio $U_s\alpha/c_0$—for example, for $\alpha = 25$ and a surface wind cycle of amplitude 5 m s^{-1}, the standard deviation of U_s would be $\sigma_j/5$ m s^{-1}.

2) The mean of the expected values of the maximum excursion (M_T) of the random walk is

$$E|M_T| = \sqrt{\frac{2}{\pi}}\sqrt{T}\sigma, \qquad (40)$$

where σ is the standard deviation of the normal distribution and T is the length of the random walk.

This relation can be inverted to yield an estimate ($E|T|$) of the random walk length from the excursion (M_T), which occurred in the simulation

$$E|T| = \frac{\pi}{2}\left(\frac{M_T}{\sigma}\right)^2. \qquad (41)$$

Similar $E|T|$ were obtained if the length of the simulations was much greater than T.

The random number series were constructed using a Minitab routine, which generated a list of numbers. Individual simulations used every mth number of the list, where m was a chosen seed. The results from two lists were compared and their statistics were found to be similar.

d. Spectra

Frequency spectra for the observed temperature series and for the simulations were also obtained. In the simulation, the frequency of the random walk length $n_0 = 1/T$ was observed to mark the transition from a n^{-2} frequency dependence for $n \gg n_0$ to an approximately constant spectral density for $n \ll n_0$.

5. Results for the equilibrium model

The computational simplicity of the model allows a range of pseudoclimates to be easily investigated. We usually ran sequences of 40 000 time steps of 1 year ($h = 1$) and displayed the results for ϕ_0, ϕ_s, and U_0, with the statistics described in section 4. An ability to estimate the parameters of the model from the visual appearance of the records was rapidly acquired, and it was found to be a stimulating tool for the discussion of climate during a laboratory demonstration at the Second Australian Climate Research Graduate Summer School held at Flinders University in February 1994.

In all the runs, we set $G = 3$, $G' = 6$, and $\alpha = 25$, as discussed in section 4a. A standard deviation σ_i of 0.01 corresponds with a standard deviation of the radiation perturbation of 1 W m^{-2}, and a standard deviation σ_j of 0.01 corresponds with a standard deviation of current of 2 mm s^{-1} (section 4c).

All the results are approximately represented by the quasi-stationary expressions (35) and (36), as can be seen from Fig. 2, in which ϕ_0 and $\bar{\phi}_0$ and U_0 and $\bar{U}_0$ are essentially identical. This conclusion follows from

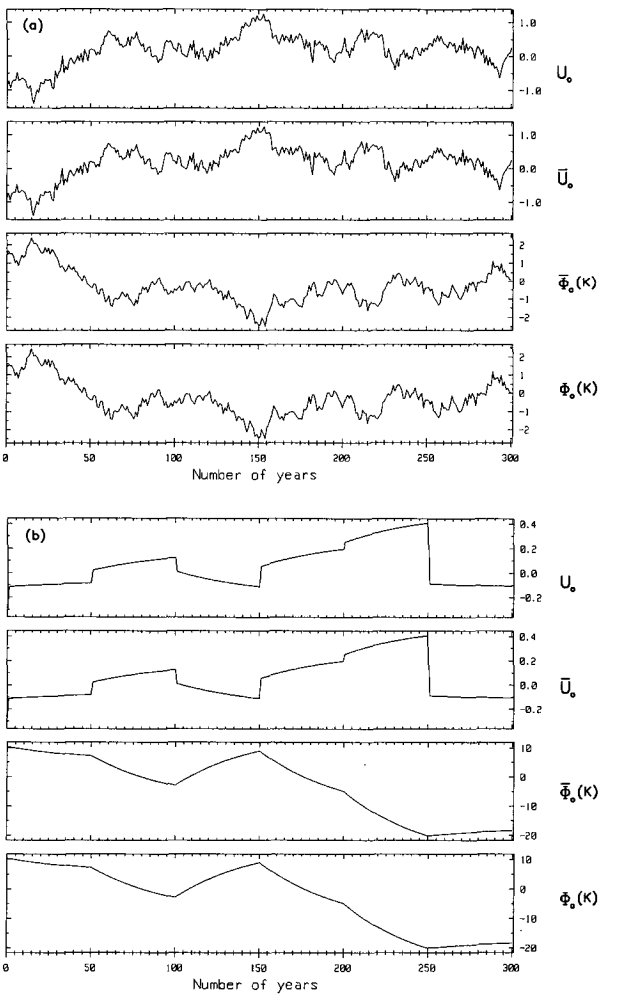

FIG. 2. 300-yr segment of run, with $H = 0.02$, $\beta = 0$ showing ϕ_0 and $\bar{\phi}_0$, and U_0 and $\bar{U}_0$. (a) $T_0 = 2$ yr, and (b) $T_0 = 100$ yr.

the transient response for ψ and λ [(A3), (A4), (A5), and (A6) of the appendix], which is negligible after 1 yr since $e^{-(G+G')/2} \sim 0.01$. In other words, the (relative) atmospheric anomalies persist for much less than a year. The exponential decay is, in fact, consistent with an atmospheric persistence of about 2 months since after 1 month, $e^{-(G+G')/24} \sim 0.7$. It is interesting that this behavior is controlled equally by the time constants for heat and momentum exchange (G and G').

Two types of simulation were run.

a. *Single frequency responses (ω-climatic regimes)*

Table 1 summarizes the statistics for atmospheric oscillations of two periods (T_0 = 2 and 100 yr), which were obtained by applying the random number sequences in blocks of time steps of length h = 1 and h = 50, respectively, and choosing H to reproduce the observed transition ratio ($\bar{r}$) for the minimum period atmospheric oscillation ($T_{\min}$ = 2 yr). This was done for (i) no current forcing ($\sigma_j/\sigma_i = 0$) and (ii) a realistic level of current forcing ($\sigma_j/\sigma_i = 0.65$) (see section 5b). We show the standard deviation of the estimates of $\bar{r}$ and the random walk length [$E(T)$] obtained from a series of five runs.

For the 2-yr oscillation, the group (i) results indicate that in order to achieve the observed value of $\bar{r}$, without any contribution to the variance from the current forcing, the thermal e-folding time with the deep ocean (H^{-1}) is very short (1.8 yr), and the random walk length is about 25 years. The group (ii) results illustrate the effect of the current forcing, for which $\bar{r} = -0.5$ (see section 4b). It is clear that the observed value of $\bar{r}$ can be obtained by combining the radiative and current variance and that in this situation the thermal e-folding time and random walk lengths are much greater. For ($\sigma_j/\sigma_i = 0.65$), we have H^{-1} = 50 yr and $E(T) \sim 250$ yr. It is found that a modest further increase in σ_j/σ_i greatly increases the random walk lengths, which become unbounded when $\sigma_j/\sigma_i = 0.75$. Figure 2(a) illustrates the random walk behavior of the group (ii) run and also the short period interannual variability. The inverse relation between $\bar{\phi}_0$ and $\bar{U}_0$ during random walk excursions, which is predicted by (34), is clearly observed.

The 100-yr oscillation runs are characterized by positive $\bar{r}$ (Table 1) due to slowly varying trends in adjustment to the random number forcing, as shown by the group (ii) run (Fig. 2b).

TABLE 1. Statistics of single frequency runs. In all runs, N = 40 000, G = 3, G' = 6, and α = 25.

T_0	H	$\bar{r}$	$E\|T\|$	σ_i	σ_j
2	0.55	−0.279 ± 0.002	23 ± 3	0.01	0
100	0.55	0.597 ± 0.001	—	0.01	0
2	0.02	−0.272 ± 0.004	237 ± 30	0.01	0.0065
100	0.02	0.949 ± 0.001	—	0.01	0.0065

TABLE 2. Statistics of multiple period forcing runs. In all runs, N = 40 000, σ = 0.125 K, G = 3, G' = 6, and α = 25.

H	$\bar{r}$	$E\|T\|$	σ_i	σ_j	β
1.1	−0.279 ± 0.005	22 ± 1	0.0055	0	0
0.6	−0.290 ± 0.015	35 ± 3	0.0043	0.0028	0
0.07	−0.281	144	0.0034	0.0038	0
0.01	−0.286 ± 0.015	551 ± 100	0.0032	0.0039	0
0	−0.275	(40 000)	0.0034	0.0040	0
0.55	−0.263	164	0.0038	0	0.025
0.07	−0.272	175	0.0034	0.0038	0.025

b. *Multiple period forcing (interannual climatic variability)*

In section 3d, it was observed that the energy spectrum of the white noise in period space was of the form in (38). In order to implement this result in the runs, a simple procedure was adopted whereby the random sequence R was partitioned into subsequences R^i_{i-1}, which comprised the variance in the averaging interval (h^i, h^{i-1}), the minimum interval being h^0 = 1 and the maximum being $h^n = N$, where N is the number of time steps in the run.

The sequence h^i, i = 0, n was selected on an ad hoc basis, bearing in mind that the response of the system is strongly dependent on the period of the atmospheric oscillation, and that adopted for the runs was h^i (i = 0, 6); 1, 3, 10, 30, 100, 300 and N, which were used to excite atmospheric variability (ω climatic regimes) of periods T_0 = 2, 6, 20, 60, 200, and 600 yr. Figure 3 shows the cumulative variances (σ_0^2) obtained from such a sequence of unit total variance, which are well represented by the relation (38). The important feature is the sharp reduction in variance with period. The summation of this sequence of ω climatic regimes represents the interannual climatic variability. The integrated result was found to not be very sensitive to the choice of sequences of similar length and distribution.

Table 2 shows the statistics of runs with five values of H, each of which has been tuned to give approximately the observed value of $\bar{r}$, and also σ = 0.125 K. It is apparent that H decreases and the random walk length increases with an increase in the ratio (σ_j/σ_i). A maximum ratio is obtained when H = 0, at which point there is no heat exchange with the deep ocean and the random walks are unbounded.

The "climate" for the maximum value of H (thermal e-folding time of 0.9 yr), which can support the observed value of $\bar{r}$, appears to be almost stationary (Fig. 4), and the variability of ϕ_0 and ϕ_s is almost identical. As the ratio (σ_j/σ_i) increases, the random walk length initially changes gradually since the system is controlled essentially by the radiation perturbations.

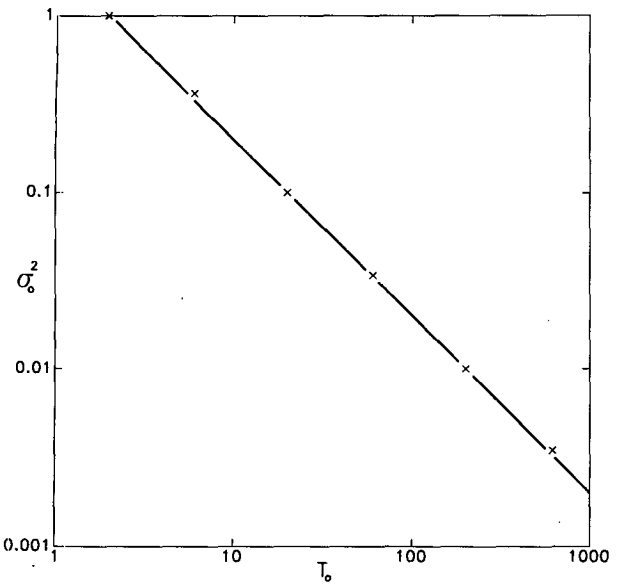

FIG. 3. Cumulative variance (σ_0^2) with period (T_0) for the set of periods used in the white noise forcing.

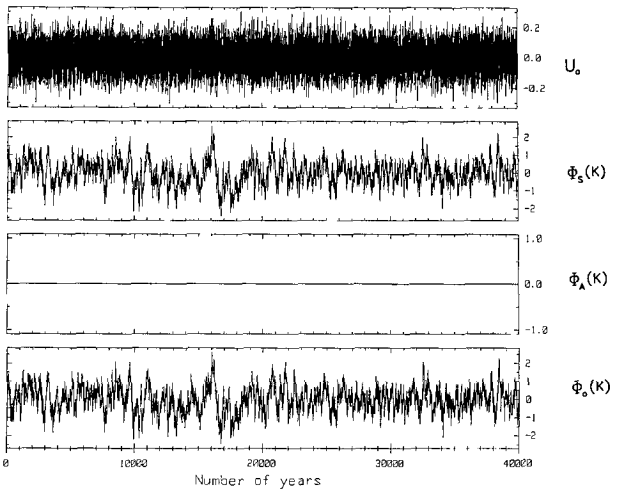

FIG. 5. 40 000-yr run, with $H = 0.01$ and $\beta = 0$.

For example, for an e-folding time of 17 yr, the random walk length has only increased to 35 yr. For a small extra increase in (σ_j/σ_i), however, a change occurs, and the system is controlled by the balance of the radiation and the current perturbations (see section 4b). In this regime, the random walk lengths increase sharply for a small change in (σ_j/σ_i) and become unbounded for $\sigma_j/\sigma_i \sim 1.2$ when the heat exchange with the deep ocean has become negligible.

Figure 5 shows the run for $H = 0.01$. Its character is totally different from that of the $H = 1.1$ run, with well developed excursions—for example, between 16 000 and 17 000 yr, during which period the mean air temperature falls by 4 K. The long-period appearances of the ϕ_0 and ϕ_s signals are again very similar, the additional variance in ϕ_0 being attributed to short-period events as shown, for example, in Figure 6.

A subjective impression suggests that the observed climate lies somewhere between the two illustrated runs (Figs. 4 and 5). Figure 6 is an expanded segment of a run with an intermediate random walk length of 144 years and a thermal e-folding time with the deep ocean of 14 years. The air temperature signal on a short-period scale is characterized by a structure, in which oscillations suggestive of quasi-biennial (QBO) and El Niño–Southern Oscillation (ENSO) events (Rasmussen et al. 1990) occur. Superimposed on this ensemble is a random walk. The additional structure on the ϕ_0 signal, in comparison to the ϕ_s signal, is due to

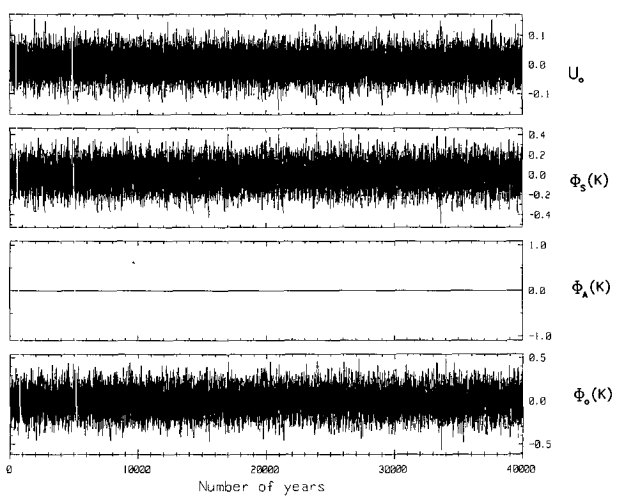

FIG. 4. 40 000-yr run, with $H = 1.1$ and $\beta = 0$.

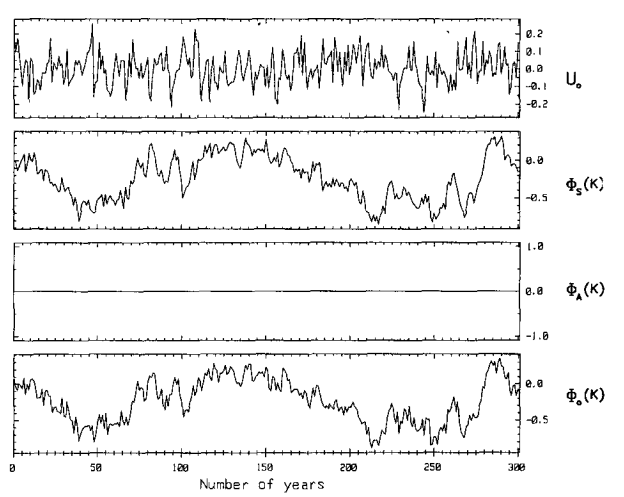

FIG. 6. 300-yr segment of run with $H = 0.07$, $\beta = 0$.

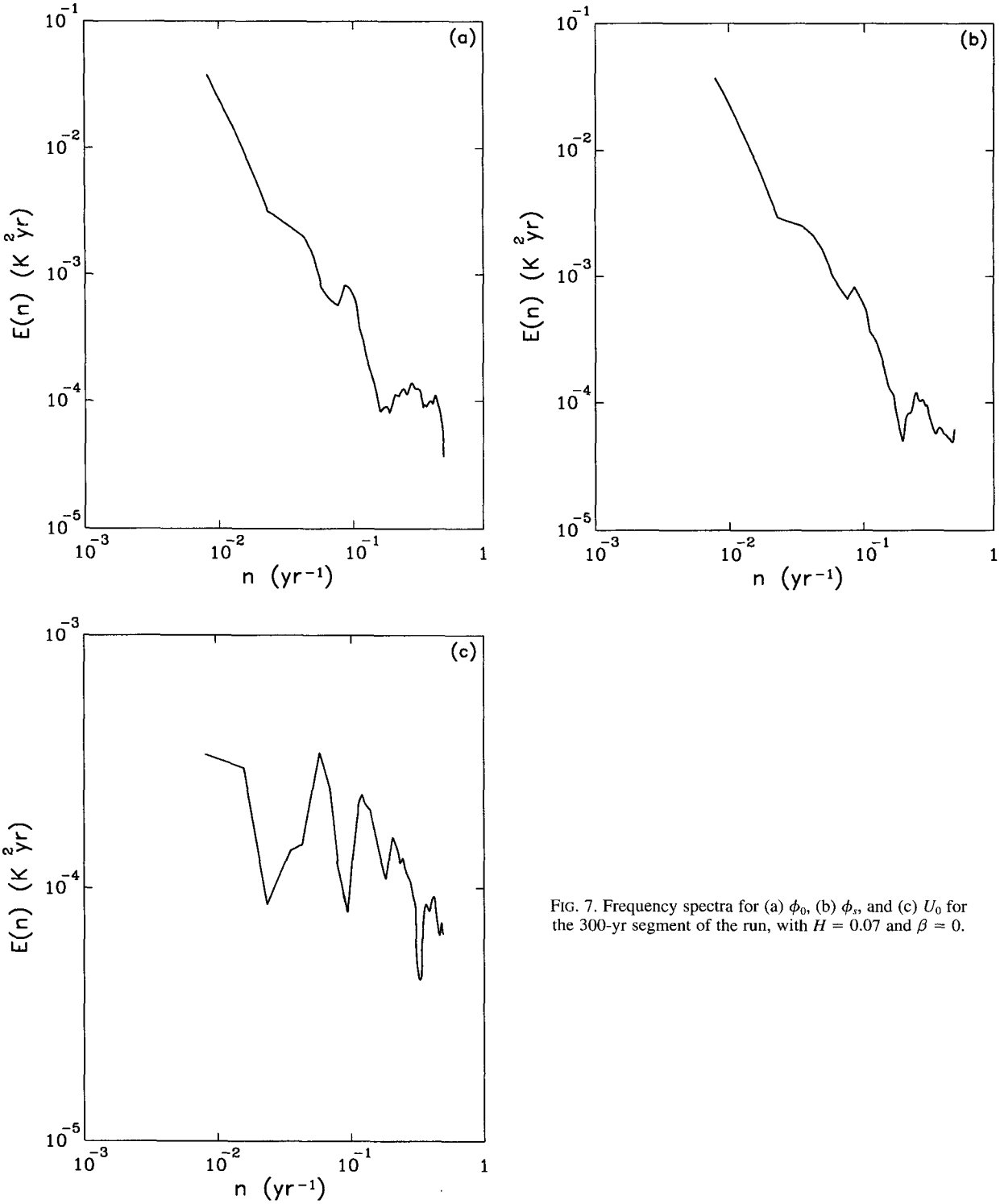

FIG. 7. Frequency spectra for (a) ϕ_0, (b) ϕ_s, and (c) U_0 for the 300-yr segment of the run, with $H = 0.07$ and $\beta = 0$.

the surface wind variability, which is seen to be almost stationary.

In the limit in which the radiation perturbations are negligible, (33) would predict that $\bar{\phi}_0$ and $\bar{U}_0$ are in phase, in contrast to the limit discussed in section 3c, in which the radiation perturbations dominate and $\bar{\phi}_0$ and $\bar{U}_0$ are out of phase. The quasi-stationary expression for $\bar{U}_0$, (36), shows that the stationary ap-

pearance of the U_0 time series (Figs. 5 and 6) is due to the dominance of the U_s forcing at low frequencies.

The energy spectra obtained from the expanded segment of 300 yr (Fig. 7) show structure attributable to the short length of the record. The air and sea temperature anomalies, however, indicate an approximate -2 frequency dependence with additional high-frequency energy being present in the ϕ_0 spectrum. There is a clear similarity between the ϕ_0 spectrum and the spectrum of the global temperature series (Fig. 8), which also shows ranges of approximately -2 frequency dependence and a shoulder at about $n = 0.1\ \text{yr}^{-1}$.

For the complete run of 40 000 yr, the ϕ_0 and ϕ_s spectra (Fig. 9) show very well defined -2 frequency ranges for $n > n_0$, where n_0^{-1} is approximately the random walk length of 150 yr. For $n > n_0$, the energy density is approximately constant. There is no clear indication of peaks associated with any of the discrete periods of the multiple period forcing. The wind anomaly spectrum has a different character (Fig. 9), with several energy peaks (also not obviously associated with the multiple-period forcing) and no well-developed -2 frequency range. The quasi-steady expression for $\bar{U}_0$, (36), shows the reason for this structure. At low frequencies, U_0 is dominated by the stationary forcing (U_s) (as discussed above), whereas ϕ_0 is dominated by the random walk forcing (ϕ_s), [see (35)].

In Gordon and Bye (1993), the global temperature series (T_k) was also filtered using the exponential filter

$$\hat{T}_k = \frac{\left(\sum_{i=0}^{i=n} T_{k-i} e^{-i/\tau}\right)}{\left(\sum_{i=0}^{i=n} e^{-i/\tau}\right)}; \quad n = 5,$$

in which τ is a decay time in years, $\hat{T}_k$ is the filtered series, and τ was chosen so that $\hat{T}_k$ had the random walk property that $\bar{r} = 0$ and the difference series ($T'_k = T_k - \hat{T}_k$) had the stationary property that $\bar{r} = -0.5$. For the global temperature series, we found that $\tau = 0.85 \pm 0.1$ yr. Figure 10 shows the filtered and difference series for a 300-yr segment of the $H = 0.07$ run, for which $\tau = 0.83$ yr. In Gordon and Bye (1993), the filtered series was called the random component of the signal and the difference series the predictable component. From this analysis, we interpret the predictable component as that which would arise if ocean heat storage anomalies are neglected.

The observed values of the transition ratio ($\bar{r}$) and the associated decay time (τ) are probably not a property of the exchange parameters G, G', and α. Rather, they are determined by the allowable short-period interannual oscillations that are supported by the coupled ocean–atmosphere. This idea was suggested in Gordon and Bye (1993), in which it was shown that the magnitude of τ was consistent with the existence of oscillations of natural integral periods of up to about four years—that is, QBO and ENSO signals.

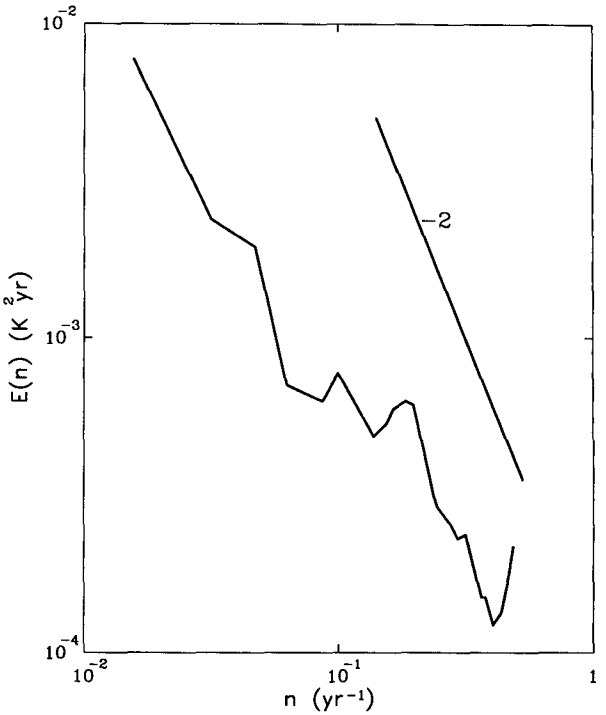

FIG. 8. Frequency spectrum of the annual global temperature series.

The partition of variance between the filtered and difference air temperature signals is in the ratio 0.0072:0.0026, which is very similar to that for the observed global temperature series of 0.0069:0.0025 (Gordon and Bye 1993). This indicates that about three-fourths of the variance is derived from ocean heat storage anomalies, the remainder being from equilibrium heat and momentum exchange fluxes.

6. The transient model

The equilibrium ("slab" ocean) model can be easily extended to include an active deep ocean. For a deep ocean of finite heat capacity, ϕ_s is replaced by $(\phi_s - \phi_A)$ and ϕ_0 by $(\phi_0 - \phi_A)$, such that (14) becomes

$$\frac{d(\phi_s - \phi_A)}{dt} + H(\phi_s - \phi_A) = \frac{G}{B} q \qquad (42)$$

and the deep ocean temperature (ϕ_A) satisfies the equation

$$\frac{d\phi_A}{dt} = H\beta(\phi_s - \phi_A), \qquad (43)$$

where $\beta = D/D_0$, in which D is the depth of the mixed layer and D_0 is the depth of the deep ocean below the mixed layer.

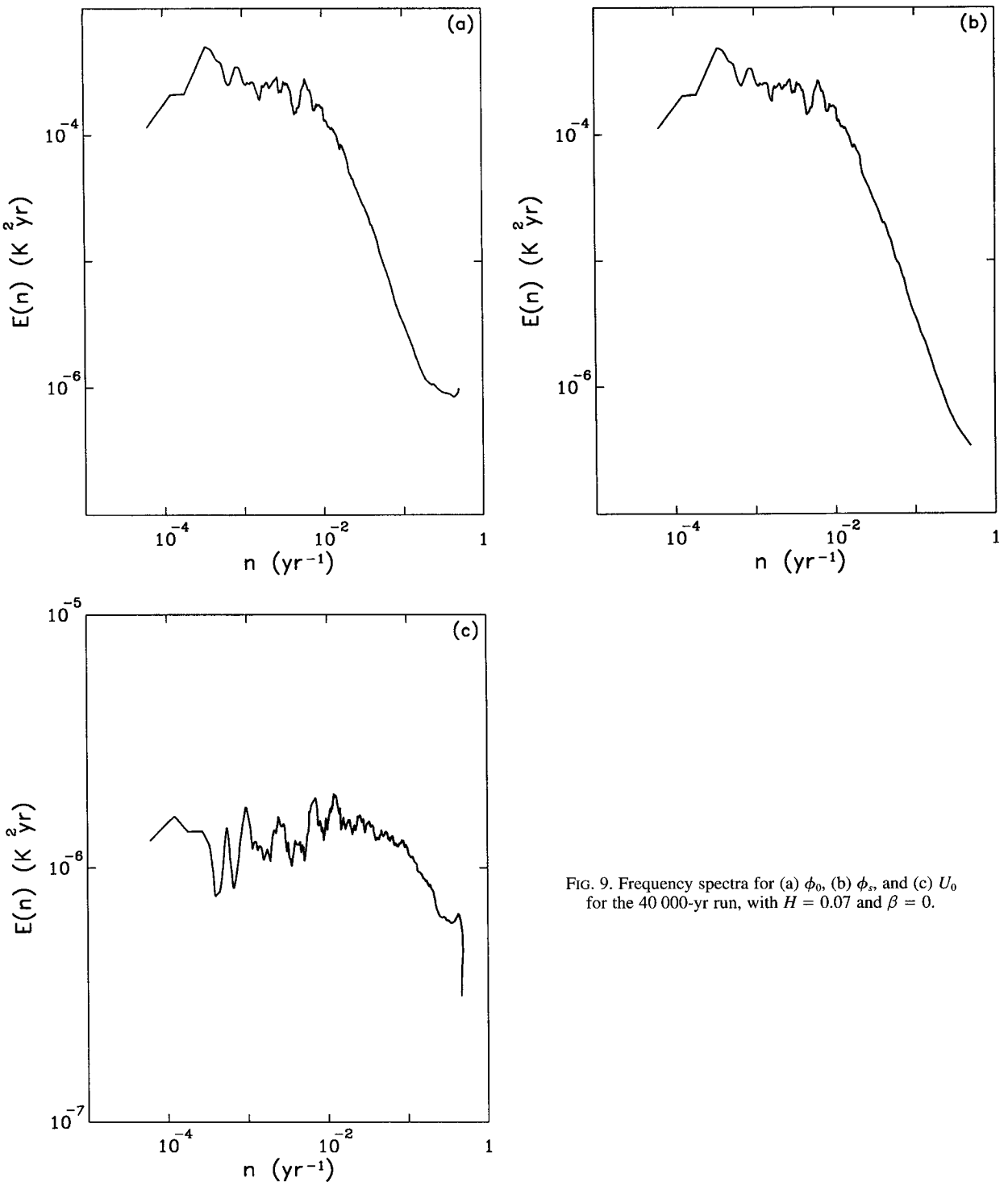

FIG. 9. Frequency spectra for (a) ϕ_0, (b) ϕ_s, and (c) U_0 for the 40 000-yr run, with $H = 0.07$ and $\beta = 0$.

The solution of this pair of equations for $q = iq_0$ is

$$\phi_s = \phi_A + \frac{iq_0}{H}\frac{G}{B}(1 - e^{-Ht}) + (\phi_{s0} - \phi_{A0})e^{-Ht}, \tag{44}$$

where

$$\phi_A = \phi_{A0}[1 - \beta(1 - e^{-Ht})] + \phi_{s0}\beta(1 - e^{-Ht}) + \frac{iq_0G}{B}\beta\left[t - \frac{1}{H}(1 - e^{-Ht})\right], \tag{45}$$

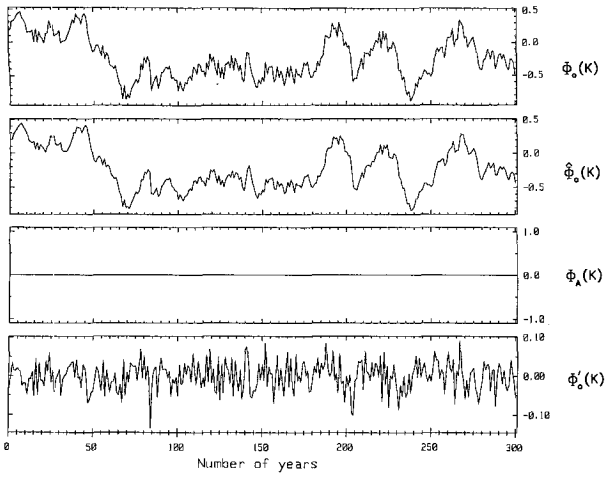

FIG. 10. Air temperature (ϕ_0), filtered air temperature ($\hat{\phi}_0$), and difference air temperature ($\phi_0' = \phi_0 - \hat{\phi}_0$) series, obtained from the 300-yr segment of a run, with $H = 0.07$ and $\beta = 0$, using the decay time $\tau = 0.83$ yr.

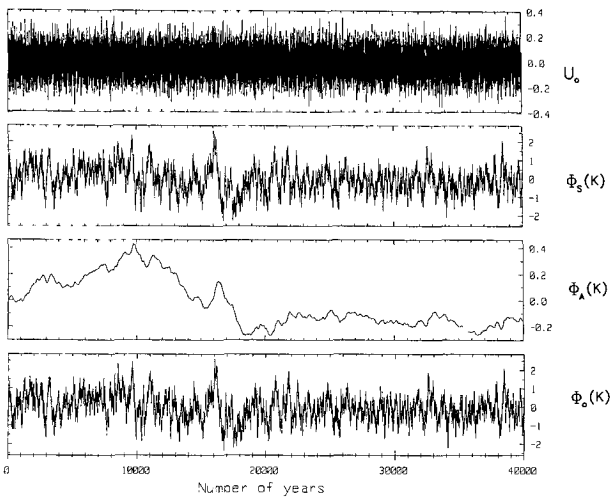

FIG. 11. 40 000 yr run, with $H = 0.01$ and $\beta = 0.025$, using the same random number seed as in Fig. 5.

in which $\phi_{s0} = \phi_s(0)$ and $\phi_{A0} = \phi_A(0)$. The linear term represents a secular heating of the mixed layer and the deep ocean, and the solutions for ϕ_s and ϕ_0 are identical to those for the equilibrium model (section 3), with the addition of ϕ_A.

For $Ht \to 0$, which is a good approximation over the interval $0 \leqslant t \leqslant h$, (44) and (45) yield the relations

$$\phi_s = \phi_{s0} - Ht(1 - \beta)(\phi_{s0} - \phi_{A0}) + \frac{Giq_0}{B} t \quad (46)$$

and

$$\phi_A = \phi_{A0} + \beta Ht(\phi_{s0} - \phi_{A0}). \quad (47)$$

In all the runs, we assume that the mixed layer depth $D = 100$ m and that the depth of the deep ocean under the mixed layer $D_0 = 4000$ m, such that $\beta = 0.025$. The annual cycle for $\beta = 0$ is not shown, but for $\beta = 0.025$ it is very similar to that for $\beta = 0$ given in section 3a.

Figure 11 shows the run for $H = 0.01$, obtained with the same random number seed as in Fig. 5. The short-period variability is very similar, but superimposed on the air and sea surface temperature signals is the deep ocean temperature signal, which exhibits a relatively smooth attenuated response that lags the sea surface temperature variability. This is due to the small heat exchange between the layers. The statistics of the runs with $\beta = 0$ and $\beta = 0.025$ are almost identical, see $H = 0.07$ (Table 2).

With no current variability ($H = 0.55$), the response is totally different, as the low-frequency responses of all the temperature fields are almost identical. This is due to the short time constant for heat exchange between the deep and surface layers. From Fig. 12, one has the impression that a change in climate occurs between 20 000 and 30 000 yr. The run statistics between $\beta = 0$ and $\beta = 0.025$ also differ, due to the role of the deep ocean (Table 2).

7. Conclusions

The elements of the world's climate have been demonstrated by a coupled analytical model, which has four main features.

(i) The atmosphere oscillates at all periods, $T_0 \geqslant 1$ yr.

(ii) The ocean stores heat.

(iii) The ocean exchanges momentum with the atmosphere.

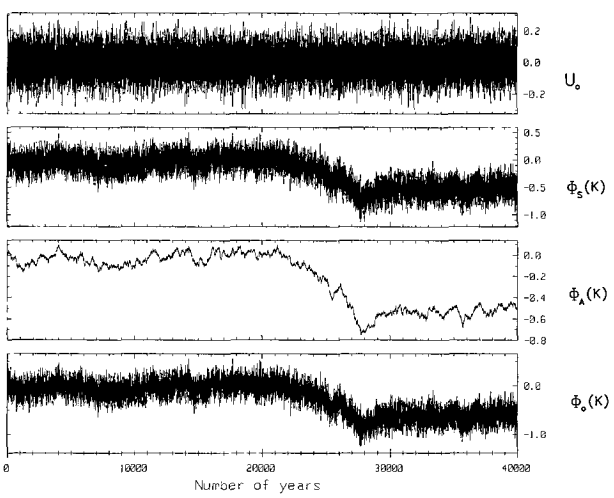

FIG. 12. 40 000 yr run, with $H = 0.55$ and $\beta = 0.025$.

(iv) Random forcing exists due to atmospheric thermodynamics and oceanic dynamics possibly associated with the global hydrological regime.

The interannual variability has been assumed throughout to be generated by random fluctuations (see section 3b); that is, discrete forcing at periods other than the annual period is not considered.

The relative importance of (ii) and (iii) in determining the climate has been assessed by reproducing the transition ratio ($\bar{r}$) for the global air temperature. We find that the climate signal can be simulated by either a relatively fast exchange of heat with the deep ocean and little ocean current variability or a slower heat exchange and greater current variability, and that the greater the current variability the more pronounced are the climatic random walks.

It is suggested that in reality these two properties, heat exchange with the deep ocean and current variability, are linked by the ocean thermodynamics. A large heat exchange coefficient with the deep ocean (H) would be expected to produce a large current variability (σ_j). Table 1 indicates, however, that the observed transition ratio ($\bar{r}$) is obtained for pairs of H and σ_j, which are in inverse relation, from which it follows that a unique combination of H and σ_j may exist. This combination cannot be determined from our algorithm, and we have used the pair $H = 0.07$ and $\sigma_j = 0.0038$ as a plausible illustration. In principle, the information on the naturally occurring combination—whether it exists, and if so, what it is—could be extracted from an oceanic general circulation model. Our analysis indicates that it is a very important number pair since it determines the extent of the random walks.

In summary, the four decay constants (of different orders of magnitude) that control the interannual variability, as represented by our algorithm, are (i) $\alpha G' \sim 10^2$—this constant is sufficiently large that its magnitude is unimportant for climate, but highly relevant for weather [see (30) and section 4a]; (ii) $G + G'/2 \sim 10$—this constant controls the persistence of the atmospheric anomalies, which is negligible on an annual scale (section 5); (iii) $1/\tau \sim 1$—this constant appears to be a property of the land/sea–air system peculiar to the present geography, and its magnitude is consistent with the observed QBO and ENSO interannual variability (see section 5); and (iv) $H \sim 10^{-1}$—this constant controls the extent of the climatic random walks, which are probably of a century-long timescale, and is of great climatic significance.

Acknowledgments. Mrs. Kim van Antwerpen assisted in obtaining the results, using the computer program for the climate algorithm. Copies of the computer program are available upon request from the authors. The manuscript was typed by Ms. Carol Howard. The project was partially funded by the Australian Research Council. Helpful comments by the referees are also gratefully acknowledged.

APPENDIX

The Piecewise Continuous Solutions for ψ and λ

The solution of (11) and (12) consists of a transient response (the complementary function) and a forced response (the particular integral) due to the random forcing in the interval. The wave equations for ψ and λ derived from (11) and (12) are

$$\frac{d^2\psi}{dt^2} + (G + G')\frac{d\psi}{dt} + (\omega^2 + GG')\psi = H\frac{d\phi_s}{dt} + (G'H - \omega^2)\phi_s + \omega\left[\frac{dU_s}{dt} + G'(1 + \alpha)U_s\right] \quad \text{(A1)}$$

and

$$\frac{d^2\lambda}{dt^2} + (G + G')\frac{d\lambda}{dt} + (\omega^2 + GG')\lambda = -\omega\left[\frac{d\phi_s}{dt} + (G + H)\phi_s\right] + G'\alpha\frac{dU_s}{dt} + (GG'\alpha - \omega^2)U_s. \quad \text{(A2)}$$

Over the interval $0 \leqslant t \leqslant h$, the transient solutions of (A1) and (A2) are

$$\psi = e^{-(G+G')/2t}\left\{\psi_0\left[\cos\sigma t + \frac{1}{\sigma}\left(\frac{G' - G}{2}\right)\sin\sigma t\right] + \frac{2\pi}{\sigma}\lambda_0 \sin\sigma t\right\} \quad \text{(A3)}$$

and

$$\lambda = e^{-(G+G')/2t}\left\{\lambda_0\left[\cos\sigma t - \frac{1}{\sigma}\left(\frac{G' - G}{2}\right)\sin\sigma t\right] - \frac{2\pi}{\sigma}\psi_0 \sin\sigma t\right\}; \quad \omega \geqslant \frac{1}{2}|G' - G|, \quad \text{(A4)}$$

in which $\sigma = (\omega^2 - \frac{1}{4}(G' - G)^2)^{1/2}$, and $\psi_0 = \psi(0)$ and $\lambda_0 = \lambda(0)$, and

$$\psi = e^{-(G+G')/2t}\left\{\psi_0\left[\cosh mt + \frac{1}{m}\left(\frac{G' - G}{2}\right)\sinh mt\right] + \frac{2\pi}{m}\lambda_0 \sinh mt\right\} \quad \text{(A5)}$$

$$\lambda = e^{-(G+G')/2t}\left\{\lambda_0\left[\cosh mt - \frac{1}{m}\left(\frac{G'-G}{2}\right)\sinh mt\right] - \frac{2\pi}{m}\psi_0 \sinh mt\right\}; \quad \omega \leqslant \frac{1}{2}|G'-G|, \quad \text{(A6)}$$

where

$$m = \sqrt{\frac{1}{4}(G'-G)^2 - \omega^2}.$$

REFERENCES

Bye, J. A. T., 1988: The coupling of wave drift and wind velocity profiles. *J. Mar. Res.,* **46,** 467–472.

——, 1995: Inertial coupling of fluids with large density contrast. *Phys. Lett. A,* **202,** 222–224.

Byers, J. R., 1974: *General Meteorology.* 4th ed. McGraw Hill, 461 pp.

Feller, W., 1962: *An Introduction to Probability Theory and Its Applications 1.* Wiley and Sons, 461 pp.

Gordon, A. H., and J. A. T. Bye, 1993: Random walk expectancies for recent global climate, and in an enhanced Greenhouse warming. *Global and Planetary Change,* **8,** 181–188.

Hasselmann, K., 1976: Stochastic climate models Part I, Theory. *Tellus,* **28,** 473–485.

IPCC, 1992: Climate Change 1992. *The Supplementary Report to the IPCC Scientific Assessment,* Cambridge University Press, 96–134.

Johnson, G. C., and H. L. Bryden, 1989: On the size of the Antarctic Circumpolar Current. *Deep-Sea Res.,* **36,** 39–53.

Jones, P. D., T. M. L. Wigley, and G. Farmer, 1991: Marine and land temperature data sets: A comparison and a look at recent trends. *Greenhouse-Gas-Induced Climate Change: A Critical Appraisal of Simulations and Observations,* M. E. Schlesinger, Ed., Elsevier, 153–172.

Manabe, S., R. J. Stouffer, M. J. Spelman, and K. Bryan, 1991: Transient responses of a coupled ocean–atmosphere model to gradual changes of atmospheric CO_2. Part 1: Annual mean response. *J. Climatol.,* **4,** 785–818.

Rasmussen, E. M., X. Wang, and C. F. Ropelewski, 1990: The biennial component of ENSO variability. *J. Mar. Syst.,* **4,** 71–96.